Investigation on laser–plasma coupling in intense, ultrashort irradiation of a nanostructured silicon target

2014 Plasma Phys. Control. Fusion 56 095001

(http://iopscience.iop.org/0741-3335/56/9/095001)

IOP Publishing Plasma Physics and Controlled Fusion

Plasma Phys. Control. Fusion **56** (2014) 095001 (10pp) doi:10.1088/0741-3335/56/9/095001

Investigation on laser–plasma coupling in intense, ultrashort irradiation of a nanostructured silicon target

G Cristoforetti[1], A Anzalone[2], F Baffigi[1], G Bussolino[1], G D'Arrigo[3], L Fulgentini[1], A Giulietti[1], P Koester[1], L Labate[1,4], S Tudisco[2] and L A Gizzi[1,4]

[1] Intense Laser Irradiation Laboratory (ILIL), INO-CNR, Via G.Moruzzi 1, 56124 Pisa, Italy
[2] INFN—Laboratori Nazionali del Sud, via S. Sofia 62, 95125 Catania, Italy
[3] Istituto per la Microelettronica e Microsistemi, CNR, VIII strada 5, 95121 Catania, Italy
[4] INFN, Pisa Section, Largo B. Pontecorvo 3, 56127 Pisa, Italy

E-mail: gabriele.cristoforetti@cnr.it

Received 4 March 2014, revised 5 May 2014
Accepted for publication 27 May 2014
Published 24 June 2014

Abstract

One of the most interesting research fields in laser–matter interaction studies is the investigation of effects and mechanisms produced by nano- or micro-structured targets, mainly devoted to the enhancing of laser–target or laser–plasma coupling. In intense and ultra-intense laser interaction regimes, the observed enhancement of x-ray plasma emission and/or hot electron conversion efficiency is explained by a variety of mechanisms depending on the dimensions and shape of the structures irradiated. In the present work, the attention is mainly focused on the lowering of the plasma formation threshold which is induced by the larger absorptivity.

Flat and nanostructured silicon targets were here irradiated with an ultrashort laser pulse, in the range 1×10^{17}–2×10^{18} W μm^2 cm^{-2}. The effects of structures on laser–plasma coupling were investigated at different laser pulse polarizations, by utilizing x-ray yield and $3/2\omega$ harmonics emission. While the measured enhancement of x-ray emission is negligible at intensities larger than 10^{18} W μm^2 cm^{-2}, due to the destruction of the structures by the amplified spontaneous emission (ASE) pre-pulse, a dramatic enhancement, strongly dependent on pulse polarization, was observed at intensities lower than $\sim 3.5 \times 10^{17}$ W μm^2 cm^{-2}. Relying on the three-halves harmonic emission and on the non-isotropic character of the x-ray yield, induced by the two-plasmon decay instability, the results are explained by the significant lowering of the plasma threshold produced by the nanostructures. In this view, the strong x-ray enhancement obtained by s-polarized pulses is produced by the interaction of the laser pulse with the preplasma, resulting from the interaction of the ASE pedestal with the nanostructures.

Keywords: laser–plasma interaction, ultrashort laser, nanostructured target, two-plasmon decay

(Some figures may appear in colour only in the online journal)

1. Introduction

The advent of chirped pulse amplification (CPA) lasers enabled the investigation of laser–plasma interaction at intensities where electron dynamics is dominated by relativistic effects. The onset of this regime is approximately located at values of the normalized momentum of quivering electrons $a_0 = eE/m\omega_0 c = 0.85(I_{18}\lambda^2)^{1/2}$ around 1, where laser intensity I_{18} is expressed in units of 10^{18} W cm^{-2} and the wavelength λ in units of microns. The investigation of laser–plasma coupling at these intensities is motivated by a large amount of potential applications and by the presence of many still open issues in this field of physics. Typical aims of this kind of experiments are the optimization of plasma-based sources of high-energy x-rays or particles, for example, bunches of electrons or protons, the feasibility study of inertial

confinement fusion schemes or the investigation of properties of warm dense matter, which is of relevance for laboratory astrophysics.

Aiming at enhancing the laser–plasma coupling, in recent years, a large effort was dedicated to testing targets containing micro- or nanostructures, which in many cases, have given evidence of a larger absorptivity of laser radiation and of an enhancement of bremsstrahlung or Kα x-ray yield, one to two orders of magnitude higher than that obtained by standard flat targets [1–12], and of a higher amount and temperature of the hot electrons generated [4, 13–16]. The mechanisms able to produce an enhancement of the absorptivity of a nano- or micro-structured target can be various, depending on the geometry and dimensions of the structures. This includes the enhancement of the local electric field due to the 'lightning rod' effect at the tip of nanocolumns or to the presence of Mie plasmonic resonances in the absorption spectrum [1, 2, 7, 9–11, 17–19], the enhancement of local fields or the multi-reflections in the target cavities [2, 20] and the reduced lateral heat conduction into the target [21]. An interesting effect, resulting from the irradiation of a nanowires target with an ultrashort pulse, is that the absorption becomes volumetric rather than restricted at the material skin depth or at the critical density surface, producing an ultrahot dense plasma [22]. As a side effect, the enhanced laser–target coupling is expected to produce a lowering of the ablation/plasma formation threshold. This is relevant when using CPA pulses at high irradiance values because low intensity precursor radiation typical of these laser pulses may play a role in the interaction, producing a precursor plasma. In this case, the laser main peak interacts mainly with this plasma, rather than with a cold solid. The lowering of the plasma threshold obtained with structured targets can provide the formation of a preplasma at lower laser intensities and increase the (pre)plasma scale length, changing significantly the laser–plasma coupling. Moreover, the presence of micro-structures can result in a spatial modulation of the critical density surface. These effects can strongly modify the effectiveness of mechanisms of laser absorption like resonance absorption (RA) or vacuum heating (VH) and will be sensitive to laser beam polarization.

In view of the above, it is interesting and necessary to monitor the preplasma formation for different target structures. Such a task is hardly achievable both by using interferometric techniques, because of the needed spatial resolution, and of the difficulty to resolve high densities with visible light, or even by hydrodynamic modeling, which often fails at laser irradiances near the plasma threshold. Moreover, non-linear effects in laser light absorption, which play a fundamental role in the case of structured targets, can hardly be modeled by currently established laser ablation codes. On the other hand, the interaction of a laser pulse with a suitable scale length preplasma can produce parametric instabilities, such as stimulated Raman scattering (SRS) or two-plasmon decay (TPD), occurring at densities near $n_c/4$, where n_c is the critical density for the laser radiation. This suggests that the detection of SRS or TPD can be used as an indirect marker of the preplasma presence. The detection of $3/2\omega_0$ harmonic (where ω_0 is the angular frequency of the laser pulse), originating from the frequency mixing of a laser photon with a plasmon produced at $n_e \approx n_c/4$, constitutes a rapid and easy method to recognize the occurrence of TPD (or in particular experimental geometries of SRS) [23]. Investigating the emission of $3/2\omega_0$ harmonic with intense ultrashort laser pulses, Veisz *et al* [24] and Tarasevitch *et al* [25] showed that at intensities approaching 10^{18} W cm^{-2}, the TPD (and SRS) instability threshold is already reached for a plasma scale length $L = n_e\,(\mathrm{d}n_e/\mathrm{d}x)^{-1}$ at the density $n_c/4$ of the order of the laser wavelength λ_0. Besides, they showed that the $3/2\omega_0$ harmonic is not detected for scale lengths L shorter than $\sim \lambda_0$. A similar result was obtained by Li *et al* [26] by focusing a 100 fs laser pulse in the range 0.5–5 $\times$ 10^{18} W μm^2 cm^{-2} at different contrast ratios on a Cu plate. In the same work, particle-in-cell (PIC) simulations confirmed the experimental results showing that $3/2\omega_0$ emission begins to be visible at a preplasma scale length L of the order of the laser wavelength and disappears for $L > 4\lambda_0$. Similar PIC results have been obtained by Dong *et al* for an ultrashort pulse at 5×10^{16} W μm^2 cm^{-2} [27]. The different irradiation conditions utilized in these experiments and simulations, with intensities in the range 5×10^{16}–1×10^{19} W μm^2 cm^{-2}, suggest that this threshold does not depend on the laser intensity and therefore it cannot be explained on the basis of the exponential growth rate $\exp\left[\gamma(I, L)\tau\right]$ of the instability. Rather, the threshold seems to depend on a different effect intrinsically related to the length of laser or plasmon wavelength. Veisz *et al* [24], after discussing the potential effects of saturation, plasmon propagation and laser absorption on the TPD threshold, concluded that none of these effects can explain the abrupt change of $3/2\omega_0$ signal at $L \approx \lambda_0$ and suggested that no $3/2\omega_0$ signal is generated as long as the active region is smaller than the plasmon wavelength (which is of the same order of magnitude as the laser wavelength). Relying on these observations, we here use the detection of $3/2\omega_0$ emission as an indirect indicator of the presence of a preplasma of scale length $L > \lambda_0$ at the $n_c/4$ layer.

The present work is focused on the investigation of the effects of a nanostructured target surface in ultrashort laser–plasma interaction at intensities near the relativistic threshold, in the range 10^{17}–2×10^{18} W μm^2 cm^{-2}.

For this scope, the x-ray emission produced by the interaction of an intense 40 fs Ti:sapphire laser pulse with a target formed by silicon nanowires was compared with that produced by using a flat silicon target. Different polarizations of the incident laser beam, resulting in the quivering of the electrons along or across the nanowires, were tested. By measuring the three-halves harmonic, the effect of nanostructures on the threshold for the formation of the preplasma is also monitored. The observed x-ray emission, measured at different observation angles, and its dependence on the laser irradiance, are discussed in terms of which mechanisms of laser–plasma coupling dominate when flat or structured targets are used.

2. Experimental setup and methodology for preplasma assessment

The experiment was carried out at ILIL laboratory in Pisa, by using a Ti : Sapphire CPA laser system, delivering 792 nm,

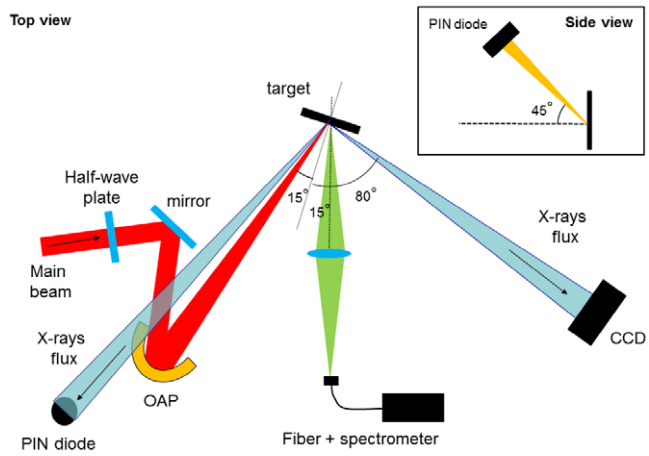

Figure 1. Experimental setup.

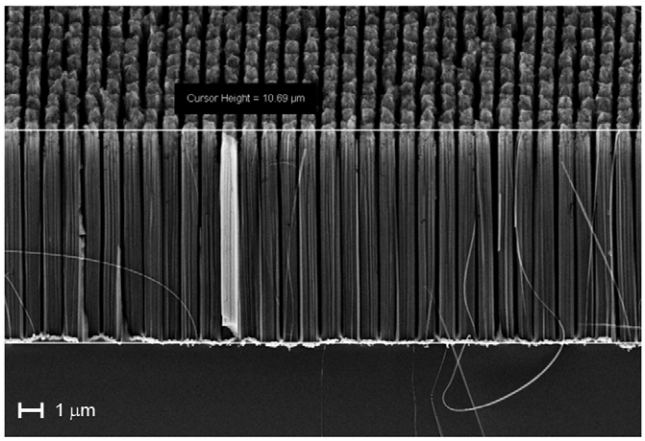

Figure 2. SEM of the nanostructured target. $3/2\omega_0$ harmonic detection for investigating preplasma formation: validity of the approach

40 fs laser pulses at a maximum energy of 120 mJ (3 TW). The laser beam was focussed on the target surface to a spot of 10 μm full width at half maximum (FWHM) by means of an effective $f/5$ off axis parabolic mirror. The angle of incidence of the beam was 15° with respect to the target normal. The quality parameter M^2 of the beam was ∼1.7 and the contrast ratio of the amplified spontaneous emission (ASE) pedestal with respect to the main peak was $\sim 4 \times 10^{-8}$. The laser irradiance on the target at the best focus was $I\lambda^2 \sim 2 \times 10^{18}$ W μm^2 cm^{-2}, where the main peak was therefore preceded by a ∼3 ns Gaussian ASE emission at $\sim 8 \times 10^{10}$ Wμm^2 cm^{-2}.

Since the laser–plasma coupling is expected to depend on the direction of the electron quivering with respect to the geometry of the structures over the target, both p- and s-polarized pulses were utilized, where the beam polarization was varied by means of a half-wave thin plate, located after the pulse compressor.

The x-ray yield was measured by means of a x-ray PIN diode and a back-illuminated cooled charged coupled device (CCD) camera (Princeton Instruments) used in single-counting mode. The CCD was located on the plane of incidence at an angle of ∼80° with respect to the target normal while the x-ray PIN diode was placed outside the plane of incidence, at an angle of ∼45° from the laser axis, as shown in figure 1. The position of the x-ray detectors was chosen with the aim of detecting non-isotropic effects of the x-ray emission due to the beam polarization.

The x-ray flux reaching the CCD was attenuated by mylar foils to preserve the condition of single-photon detection (number of photons/pixel $\ll 1$). The spectral sensitivity of the PIN diode and the CCD (including the filters) has a peak around 6 keV and 4 keV respectively and is >10% of peak sensitivity in the range 3–19 keV and 3–16 keV, respectively, which makes the comparison of their signals significant.

X-ray spectra in the range ∼10–25 keV (where sensitivity is larger than 1%) were obtained by processing CCD acquisitions in a single-photon regime [28–30]. Spectra were derived by considering the histogram of single pixel events (after applying a rejection threshold to remove the contribution of noise), and corrected by a wavelength-dependent correction curve. The curve of correction was calculated by comparing the experimental intensities of several ^{237}Np lines emitted by an ^{241}Am radioactive source with their expected transition rates [31]. This method, although significantly narrowing the spectral range, allows a reliable calibration of the detector.

The radiation in the visible range emitted specularly to the incident laser light was collected by an optical system in a solid angle of 20° and sent to a compact spectrometer by an optical fiber. Optical spectra provided by the spectrometer ranged between 200 nm and 800 nm, including the 2nd (λ ∼400 nm) and three-halves harmonics (λ ∼533 nm) of the laser light with a spectral resolution of ∼0.3 nm.

Measurements were taken for flat polished silicon targets and plane nanostructured silicon targets. A scanning electron micrograph (SEM) of the nanostructured target is shown in figure 2. Its surface consists of pillars of ∼10 μm height and 1 μm diameter regularly distributed in a grid and separated by 200 nm gaps; the top and lateral walls of the pillars are porous surfaces with cavities of the order of tens of nanometers.

The $3/2\omega_0$ emission results from the frequency mixing of a laser photon and a plasmon produced by the onset of TPD or SRS instability in the underdense plasma region near $n_c/4$. The detection of $3/2\omega_0$ emission is here used as an indirect indicator of the presence of a preplasma of scale length $L >\sim \lambda_0$ at the $n_c/4$ layer. This is particularly useful for nanostructured targets, where non-linear absorption processes occurring in the proximity of the nanostructures can hardly be reproduced by the current laser ablation codes. In the present work, where preplasma scale length is due to ASE level and increases along with the main peak intensity, the validity of the approach relies on the results summarized above [24–27], showing that in these experimental conditions, the TPD threshold depends on the intrinsic value $L = \lambda_0$ rather than on the intensity of the main peak.

Since different laser polarizations are used, resulting in different preferential directions of $3/2\omega_0$ emission, this approach is justified if the detection apparatus is able to collect the signal in all the experimental configurations. Moreover, the validity of the approach can be tested by calculating preplasma profiles with hydrodynamic simulations in case of flat targets. Both these tasks are tackled in this section.

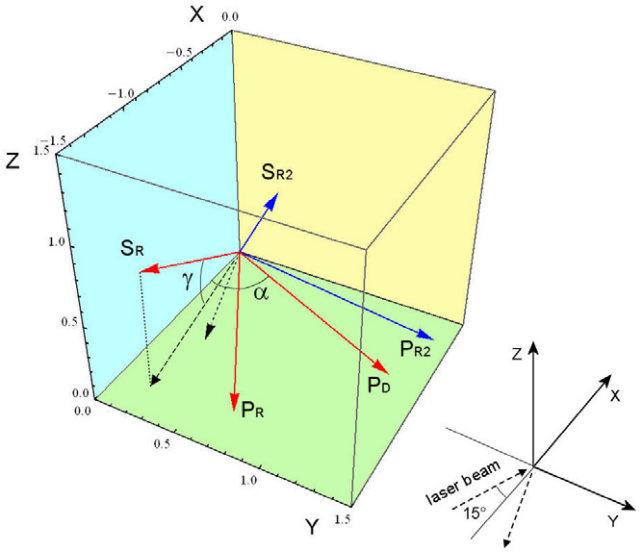

Figure 3. Geometry of laser propagation in the x–y plane and wave vectors of $3/2\omega_0$ photons produced by a TPD-induced plasmon in the case of p- and s-polarized laser beams. Wave vectors are normalized by the factor c/ω_0 and are indicated by P and S depending on laser polarization. Blue and red arrows indicate photons resulting from blue and red plasmons emitted forward and backward, respectively. $_R$ and $_D$ indicates $3/2\omega_0$ photons produced by the coupling with photons incident or reflected at critical surface. The dashed arrow indicates the direction of the reflected beam, forming an angle α of 15° with respect to the target normal.

In order to calculate the directions where $3/2\omega_0$ radiation is preferentially emitted in both p- and s-polarizations, the conditions for which the instability can develop, i.e. those dictated by energy and momentum conservation as well as by the instability growth rate, must be considered. Moreover, the formation of $3/2\omega_0$ needs a further condition, dictated by the phase matching between plasmon and e.m. wave vectors. Whenever this last condition is not fulfilled in the region where plasmons are produced, the propagation of the plasmon through the underdense plasma should be also considered. Furthermore, it should be taken into account that the plasma wave can couple both with the incoming laser photons (direct coupling) and with the photons reflected by the critical surface (reflection coupling).

By vectorial calculation in the wave vector k-space, where energy and momentum conservation as well growth rate are accounted for, the wave vectors of a $3/2\omega_0$ photon produced by a TPD-induced plasmon in case of p- and s-polarized laser beams are shown in figure 3. The wave vectors $\tilde{k}_{3/2}$ are normalized to the laser photon wave vector k_0, i.e. $\tilde{k}_{3/2} = k_{3/2}c/\omega_0$. The homogeneous plasma approximation was considered here, where inhomogeneity effects do not change the angular distribution calculated here but do effect the growth rates of the instability. The wave vectors reported in the figure represent the most favourable coupling conditions where no propagation of the plasmons is needed for the phase matching. In the graph, the normal to the target is (anti)parallel to the x axis and only the $3/2\omega_0$ photons emitted in the region $y > 0$, including the reflected beam (dashed arrow) and the collecting optics, are shown. Similarly, only the region of positive z axis is shown, considering that the semispace $z < 0$ is specular to it.

We begin our analysis by considering $3/2\omega_0$ photons produced by plasmons emitted backwards (red arrows), resulting in directions of emission downward the density gradient. P-polarized pulses result in two preferential directions, both located in the plane of incidence, produced by the coupling with the incident photons (P_D) and with those reflected at the critical surface (P_R). Their wave vectors at the $n_c/4$surface form angles α' of 29.4° and 65.6° with respect to the target normal, which become 25.1° and 52° out of the plasma due to light refraction. S-polarized beams, conversely, results in two preferential directions of $3/2\omega_0$ emission, produced by the coupling of plasmons with photons reflected at the critical surface. Their wave vectors—see S_R vector in figure 3—are symmetrical with respect to the plane $z = 0$ and located at angles $\gamma' = \pm 26.3°$ and $\alpha' = 7.3°$ with respect to the planes $z = 0$ and $y = 0$, respectively. After propagation into the plasma, $3/2\omega_0$ photons exit at angles $\gamma = \pm 22.6°$ and $\alpha = 6°$ (wave vectors in the semispace $y < 0$ are not reported in the figure). Beside these vectors, a contribution of $3/2\omega_0$ emission is expected by the TPD plasmons propagating toward the target (blue arrows). These $3/2\omega_0$ photons are emitted up the density gradient and successively reflected back toward the detecting system, as reported by the blue arrows P_{R2} and S_{R2} in figure 3. Due to the large angles of emission with respect to the spectrometer field of view, they are expected to bring a minor contribution to the measured $3/2\omega_0$ emission, as confirmed by the comparison of blue-shifted and red-shifted photons in the spectrum.

Also plasmons generated by SRS can couple with laser photons and form $3/2\omega_0$ harmonics. However, in SRS occurring at $n_e \approx n_c/4$, the laser photon transfers almost all its momentum to the plasma wave. This makes the phase matching for $3/2\omega_0$ emission much more difficult than in TPD, and requires a more oblique incidence of the laser beam, as shown by Veisz *et al* [24]. In our case, the phase coupling could be reached by considering plasmons induced at densities $n_e/n_c < 0.19$, and is favored by accounting for the plasmon propagation during the pulse. It is hard to establish the relative importance of TPD and SRS in producing the $3/2\omega_0$ harmonics. The x-ray emission data presented in the next session, however, suggests that in our conditions TPD is crucial for determining laser–plasma coupling and hot electrons emission.

Considering the closeness of P_{R2} and P_D, the wave vectors in figure 3 are in good agreement with the experimental two-peaked angular distribution of $3/2\omega_0$ emission in the incidence plane measured for p-polarized beam irradiation reported in previous literature [24, 25]. According to our calculations, a similar two-peak distribution along the plane perpendicular to the incidence plane is produced by s-polarized beams. Figure 3 also shows that the collecting optics in our apparatus, located along the laser beam reflection axis, appears not far from directions of emission indicated by P_R and S_R vectors, forming angles of ∼10° and ∼24° with the axis of signal collection. Therefore, the apparatus appears suitable for the $3/2\omega_0$ detection in both p- and s−polarizations. It is also important to remark that the experimental apparatus

preferentially detects the three-halves harmonics produced by the coupling of plasmons with the photons reflected by the critical density surface rather than that produced by the coupling with the incoming laser photons.

In our experiment, the $3/2\omega_0$ emission appears for flat targets at a laser intensity $I\lambda^2 \approx 3.5 \times 10^{17}\,\mathrm{W}\,\mu\mathrm{m}^2\,\mathrm{cm}^{-2}$, which corresponds to an ASE intensity $I\lambda^2 \approx 1.4 \times 10^{10}\,\mathrm{W}\,\mu\mathrm{m}^2\,\mathrm{cm}^{-2}$, by considering the contrast ratio of the laser system. In order to estimate the preplasma scale length at the arrival time of the main pulse, 2D hydrodynamic simulations were performed by using the POLLUX code, written by Pert [32] to model high-intensity laser irradiation ($I > 10^{10}\,\mathrm{W\ cm}^{-2}$) of solid targets. A 3 ns half width at half maximum (HWHM) Gaussian pedestal, in the range $(1.4\text{–}8.0) \times 10^{10}\,\mathrm{W}\,\mu\mathrm{m}^2\,\mathrm{cm}^{-2}$ was considered. In these conditions, only a small fraction of the laser pulse interacts with the solid target surface and plasma thermodynamics can be described by an ideal gas equation of state. Laser energy is prevailingly absorbed into the flowing outwards plasma by inverse bremsstrahlung up to the critical density surface, which is justified by the low irradiance regime. The prevalence of collisional absorption implies also that preplasma dimensions are not affected by the polarization of the ASE prepulse. Partial ionization calculated by Saha equilibrium was accounted in the simulation. The simulations show that the preplasma scale length L at $n_c/4$ is $\sim\lambda_0$ at $I\lambda^2 \approx 1.4 \times 10^{10}\,\mathrm{W}\,\mu\mathrm{m}^2\,\mathrm{cm}^{-2}$ and increases up to $\sim 3.5\lambda_0$ at $I\lambda^2 \approx 8 \times 10^{10}\,\mathrm{W}\,\mu\mathrm{m}^2\,\mathrm{cm}^{-2}$, corresponding to the maximum intensity utilized. These results are in agreement with the data reported in [24–26] and confirm the validity of our procedure.

3. Experimental results

The irradiance on the target was modified by a focal scan at steps of 50 μm and the value is calculated assuming laser pulse propagation in the focal region including the M^2 quality factor. The irradiance value onto the target spanned from 1×10^{17} to $2 \times 10^{18}\,\mathrm{W}\,\mu\mathrm{m}^2\,\mathrm{cm}^{-2}$, i.e. in the region where the relativistic effects on the electron dynamics begin to be important (a_0 in the range 0.2–1.2). For each experimental condition, the values of x-ray yield and of laser harmonics intensity were calculated by averaging 8–10 laser shots. The errors bars reported in the figures indicate statistical errors.

3.1. Preplasma formation

Figure 4 shows the comparison of the $3/2\omega_0$ emission obtained for the two types of targets and for p- and s-laser polarization. The plots show an increase of $3/2\omega_0$ emission with laser irradiance, with evidence, in some cases, of a saturation at the higher intensities. Moreover, the $3/2\omega_0$ emission obtained by s-polarized pulses is markedly higher than that obtained by p-polarized ones. A striking difference between flat and nanostructured targets is evident. While in the case of the flat Si target, no $3/2\omega_0$ signal is detected at irradiance values lower than $\sim 3.5 \times 10^{17}\,\mathrm{W}\,\mu\mathrm{m}^2\,\mathrm{cm}^{-2}$, such emission is well above the noise level down to $\sim 10^{17}\,\mathrm{W}\,\mu\mathrm{m}^2\,\mathrm{cm}^{-2}$ for nanostructured targets. As discussed above, the appearance of the $3/2\omega_0$ harmonic suggests that preplasma scale length is larger than approximately the laser wavelength λ_0, i.e. ~800 nm.

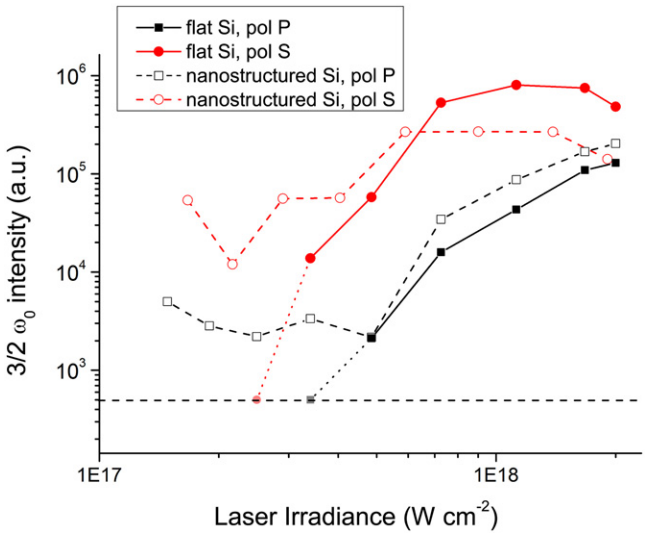

Figure 4. Spectrally integrated values of $3/2\omega_0$ emission versus laser irradiance for both targets and polarizations. Each point represents the average of 8–10 shots. The root mean square value is in the range 50–90%, where the poorest reproducibility is obtained at the lowest irradiance values. The dashed line represents the noise level, while the dotted lines represent an extrapolation of the curves obtained for flat targets, considering the absence of signal at low irradiances.

The higher signal obtained in s-polarization, which can reach at best a factor of 10 at lower laser intensities, can be partially explained by considering the role of reflected laser light. In fact, as discussed above, the three-halves harmonic emission collected by the detector is predominantly produced by the coupling of an electron plasma wave with laser light reflected at the critical surface. In the case of p-polarized pulses, RA or VH, depending on the preplasma scale length, are expected to absorb a significant part of the laser energy at the critical density surface. This reduces the intensity of the back-reflected radiation and consequently results in a reduction of the $3/2\omega_0$ emission. By considering, for example, a preplasma scale length at critical density $L_{nc} \approx 0.5\lambda_0$, as predicted by the hydrodynamic code POLLUX at the maximum laser intensity, an absorption of laser energy by RA of ~35% is expected for p-polarization. Another factor contributing to this result is that two S_R wave vectors, i.e. those in semispaces $z < 0$ and $z > 0$, are effectively measured by the experimental apparatus, while in the case of p-polarization only one emission direction (P_R) is effectively collected. Finally, also the slightly different values of plasma scale length seen by the plasma waves produced in s- and p-polarization could produce a difference between $3/2\omega_0$ intensity in the two polarizations.

The observed saturation at high laser irradiances agrees with experimental results and PIC simulations obtained by Li *et al* [26], even if they refer to a different laser incidence angle. Li *et al*, in fact, observed a reduction of $3/2\omega_0$ emission when preplasma dimensions are increased and, with PIC simulations, predicted no $3/2\omega_0$ emission for preplasma scale lengths larger than $4\lambda_0$. This value is comparable to the one found in our simulations at the maximum intensity,

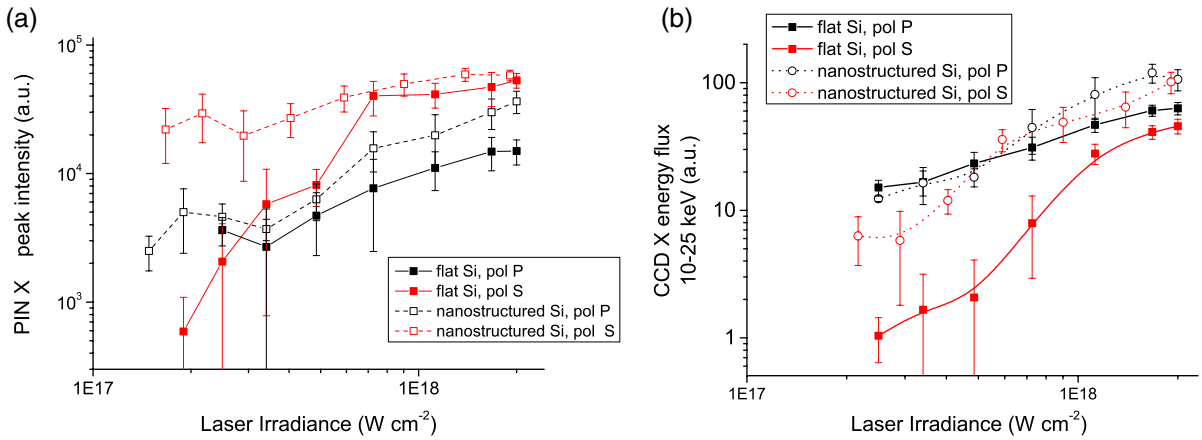

Figure 5. X-ray emission measured by the PIN X (peak intensity) (*a*) and by the CCD (energy flux) (*b*) at different laser irradiance values for flat (filled symbols) and nanowires targets (empty symbols). Black and red symbols indicate data obtained by p-polarized and s-polarized laser pulses, respectively.

i.e. $\sim 3.5\lambda_0$. The saturation (and disappearance of $3/2\omega_0$ at greater plasma scale lengths) may be due to the reduced spatial overlapping between the reflected beam and the region where instabilities develop, as suggested by Veisz *et al* [24]. At larger irradiance values, the scale length of preplasma is expected to increase, so that overlapping becomes more difficult. For example, considering a laser spot diameter of 10 μm FWHM and the laser propagation into an exponential density profile $n(x) = n_0 e^{-x/L}$, it can be calculated that the overlapping of incoming and reflected beams at $n_c/4$ vanishes at values of the density scale length L larger than $\sim 8\,\mu$m and it is approximately half of the spot size for a scale length L of 4 μm.

The experimental results show that nanostructured targets have a preplasma threshold lower at least by a factor 3 (we did not investigate laser intensities lower than $\sim 10^{17}\,\mathrm{W}\,\mu\mathrm{m}^2\,\mathrm{cm}^{-2}$), which confirms that their absorptivity is significantly larger than that of flat targets. The larger absorptivity could be due to the volumetric heating of the target [22], to the rebounds of lights between the structures or to the enhancement of electric fields in the surface cavities [2, 20]. The lower lateral heat conduction can also contribute to this result. A quantitative evaluation of these effects is a complex task because of the onset of non-linear effects needing a full quantum mechanical approach [33]. This is not in the scope of the present paper.

The different threshold of the preplasma in the two types of target will be discussed in the next section in terms of the laser–plasma interaction regime.

3.2. X-ray emission and laser–plasma interaction regime

3.2.1. Flat targets. The x-ray emission measured by the PIN diode and by the CCD at different laser intensities are reported in figures 5(*a*) and (*b*), respectively, for both flat and nanostructured targets.

Getting started from the case of flat targets, an anistropy of x-ray emission is clearly visible at the largest laser intensities. For $I\lambda^2 > 10^{18}\,\mathrm{W}\,\mu\mathrm{m}^2\,\mathrm{cm}^{-2}$, the x-ray yield measured by the CCD, which is in the plane of incidence, is in fact higher for p-polarized pulses by a factor $\sim$1.5–2. In contrast, the x-ray yield measured by the PIN diode in the orthogonal plane is larger by a factor $\sim$4–6 for the s-polarized pulses.

In another paper [34], we discussed in detail the anisotropy of x-ray emission measured in the same experimental conditions, concluding that it is mainly produced by the bremsstrahlung of hot electrons generated by the TPD process. Such hot electrons, accelerated in the plasma waves induced by TPD, are preferentially emitted in collimated jets in the plane of beam polarization, as predicted by the theory and verified by the experiments [35, 36]. Here, it is worth summarizing and discussing briefly the experimental data supporting this picture, which in the following paragraph constitutes a starting point for the interpretation of the results obtained with nanostructured targets.

Several mechanisms are able to generate suprathermal electron jets and, correspondingly, anisotropic bremsstrahlung-driven x-ray emission. Among these, the most important are ponderomotive acceleration, RA, VH, parametric instabilities, direct acceleration and laser wakefield acceleration, where each mechanism privileges particular emission directions. The effectiveness of such mechanisms depends on some experimental parameters, in particular laser intensity and polarization, preplasma scale length and laser duration.

The literature on the topic, even restricting the attention to femtosecond laser pulse interaction, reveals a complex and still debated scenario, where often a concomitance of multiple mechanisms occurs. In particular, some works [37–39] show evidence of mechanisms other than TPD, which are able to produce an anisotropic emission of hot electrons depending on laser polarization. Chen *et al* [37] and Zhang *et al* [38, 39], for example, utilizing p- and s-polarized femtosecond laser pulses revealed the presence of hot electron jets in the plane of polarization, where electrons are directly accelerated by the laser electric field. These jets, however, are obtained with a laser intensity $I = 2 \times 10^{16}\,\mathrm{W\,cm}^{-2}$ and are no longer visible at $I \approx 4 \times 10^{17}\,\mathrm{W\,cm}^{-2}$ where ponderomotive force begins to become significant. Moreover, these peaks are obtained when plasma exhibits a steep density profile and the directionality of hot electrons tends to reduce when a low density preplasma is present in front of the overdense plasma, which is explained by possible modulations of the critical

density surface. Both these features are in contrast with our results, where the x-ray directionality is observed for laser intensities larger than $\sim 3.5 \times 10^{17}$ W μm^2 cm^{-2} for which also preplasma signatures are evident. This disagreement led us to exclude direct acceleration as the cause of the observed x-ray directionality.

Our interpretation, involving the TPD instability, relies on the simultaneous measurements of $3/2\omega_0$ and x-ray emission, and on the preplasma scale length hydrodynamic simulations. As widely discussed, $3/2\omega_0$ emission is a clear signature of TPD instability and is strongly correlated with the preplasma scale length (as reported by the literature and confirmed by hydrodynamic simulations). We consider particularly relevant that the onset of x-ray directionality and of $3/2\omega_0$ emission occurs at the same laser irradiance, suggesting that x-ray anisotropy and TPD process have the same threshold intensity $I \sim 3.5 \times 10^{17}$ W μm^2 cm^{-2}, which simulations identify also as the conditions for the formation of a preplasma of a scale length of the order of the laser wavelength. In particular, x-ray directionality is related to an abrupt growth of x-ray emission in the polarization plane for s-polarized pulses. We consider the concomitance of these events as a strong indication that the two phenomena, in our experiment, are correlated.

It is worth remarking that other mechanisms of hot electron generation could be also present in our experiment. For example, it is likely that at the relativistic intensities used here ponderomotive acceleration does occur, producing an electron jet in the direction of the laser beam reflection. Our apparatus, however, is sensitive in the range of 3–25 keV, while hot electrons and consequently x-rays, estimated by ponderomotive scaling are significantly more energetic (e.g. for $a_0 = 1$ the ponderomotive hot electron temperature $T_{\rm hot} \approx 115$ keV). Similarly, RA can give a contribution to hot electrons emitted in the plane of incidence for p-polarized pulses. The concomitant presence of these mechanisms, however, results in additional hot electrons in the incidence plane and does not invalidate our interpretation.

Our picture is in agreement with PIC simulations of Sheng *et al* [40] and Zhang *et al* [38, 39], where modelling of the interaction of a femtosecond pulse with a solid target in the intensity range at 5×10^{16}–5×10^{17} W cm^{-2} in the presence of a preplasma is reported. Both works also model the visible emission spectrum, including $\omega_0/2$ and $3/2\omega_0$, and show that both SRS and TPD are responsible for the emission of hot electron jets in the presence of a preplasma. Sheng *et al* show that the jets are emitted in the plane of polarization and tend to detach from the normal to the target, approaching an angle of $\sim 50^\circ$, when preplasma scale length increases, which is due to the prevailing TPD process. Despite the slightly different conditions from our experiment, namely a lower preplasma scale length, it is reasonable that in our case, where laser intensity is larger by at least a factor four, the detachment of jets from the normal direction occurs for preplasma scale lengths which are shorter than those reported in [40]. Zhang *et al*, show that the TPD process strongly enhances laser absorption for preplasma scale lengths larger than the laser wavelength and, comparing experimental and modelling results, shows that this

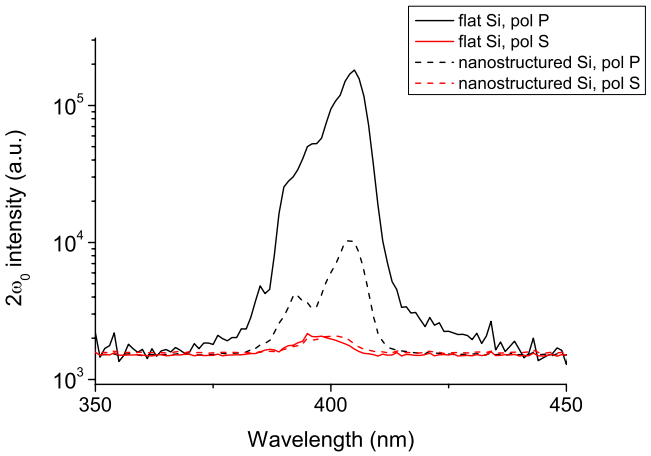

Figure 6. Spectrum of 2nd harmonic emission obtained for both the targets in p- and s-polarization at $I\lambda^2 \sim 3.5 \times 10^{17}$ W μm^2 cm^{-2}.

absorption enhancement is associated to an enhancement of x-rays and hot electrons emission. The conclusions of Zhang *et al*, reported in [37–39] are that parametric instabilities excited at quarter critical density are responsible for hot electron generation for preplasma scale length larger than the laser wavelength.

Going back to our results obtained with flat targets, the x-rays directionality disappears for intensities lower than $\sim 3.5 \times 10^{17}$ W μm^2 cm^{-2}, as shown by figure 5(*a*). The PIN X intensity obtained with s-polarized pulses in fact falls rapidly at irradiances lower than this threshold, becoming much lower than the x-ray yield obtained in the same conditions with p-polarized pulses. This can be easily explained by the inefficiency of s-polarized laser beam absorption, in conditions where the preplasma is not formed or has scale lengths too small to allow parametric instabilities to develop. Hydrodynamic simulations carried out at laser irradiance $\sim 3.5 \times 10^{17}$ W μm^2 cm^{-2} predict a scale length of $\sim \lambda_0$ at $n_c/4$, falling down to values lower than $\sim 0.1\lambda_0$ at critical density. In these conditions, p-polarized pulses can be still efficiently absorbed via VH (or Brunel) mechanism [41], which explains the higher x-ray yield obtained in this conditions. The non-zero component of e.m. oscillating field along the plasma gradient, in fact, produces a quivering of the electrons on distances larger than plasma scale length, i.e. from the overdense region to the 'vacuum' region and back, inducing plasma waves at critical density, producing a population of hot electrons and resulting in a net laser energy absorption. The above interpretation is confirmed by the spectra of the 2nd harmonic laser emission measured in the reflected beam direction at these low irradiances (figure 6). The $2\omega_0$ emission results from the interaction of the laser beam with the plasma waves produced at the critical density; it is therefore associated to RA or VH and maximized for p-polarized pulses [42]. The much higher intensity of $2\omega_0$ emission obtained with p-polarized beams with respect to s-polarized beams, confirms that RA or VH are the dominant mechanisms of laser absorption at low laser irradiances.

These results suggest that in the case of flat targets, a change of the laser–plasma interaction regime occurs at irradiances $I\lambda^2 \sim 3.5 \times 10^{17}$ W μm^2 cm^{-2}. For irradiances

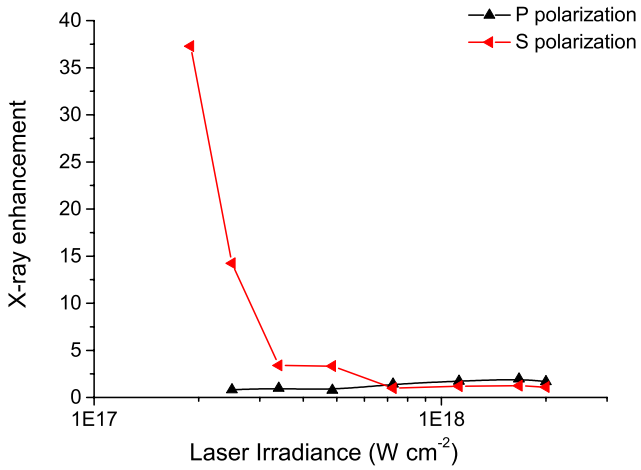

Figure 7. Enhancement of x-ray yield obtained by using nanostructured targets at different laser irradiances for p-polarized beams, in the incidence plane, and for s-polarized beams in the vertical plane.

lower than such values the laser is mainly absorbed via VH in the case of p-polarization, while it is scarcely absorbed in the case of s-polarization. In contrast, at larger irradiances, the interaction with the preplasma via the TPD process (and probably SRS) becomes important and effective in the production of hot electrons and x-rays.

3.2.2. Nanostructured targets. The effect of the nanostructures on the x-ray emission depends both on laser irradiance and polarization. The enhancement of the x-ray yield with respect to flat targets has been reported in figure 7 for the different experimental conditions used. Due to the directionality of x-ray emission in many of these conditions, the enhancement in p-polarization has been calculated by considering the signals measured on the plane of incidence while that in s-polarization from those measured in the vertical plane.

Again, a transition between different regimes is visible at $\sim 3.5 \times 10^{17}\,\mathrm{W}\,\mu\mathrm{m}^2\,\mathrm{cm}^{-2}$. At values of laser irradiance larger than this threshold, a poor enhancement in the range 1.2–2 is found for both polarizations. The lack of dependence from polarization suggests that the ASE of the pulse destroys the structures present on the surface, so that the iso-density surfaces in the plasma—as for example critical density and quarter critical density surfaces—are already plane at the arrival of the main pulse. The rough estimate of time needed by thermal ions to fill the gaps between the nanowires can be calculated by $t \approx (d/2)/v_{\mathrm{ions}}^{\mathrm{th}} = (d/2)/\sqrt{2kT/m_{\mathrm{ions}}}$, where d is the distance between the structures, $v_{\mathrm{ions}}^{\mathrm{th}}$ and m_{ions} are the thermal velocity and the mass of the Si ions. By considering a temperature of the preplasma $T = 20\,\mathrm{eV}$, a filling time of 20 ps is obtained, which is much shorter than the duration of the ASE (HWHM ≈3 ns). This confirms that the homogenization of the ion density along the target surface has already occurred at the arrival of the main pulse.

The slight increase of x-ray emission observed with nanostructured targets in this irradiance range could be produced by the different scale length of preplasma obtained with different targets, due to the different value of preplasma threshold discussed above. In particular, a larger scale length is expected for structured targets, which could make the laser energy absorption more effective—and therefore the hot electrons/x-ray production—via the TPD process.

At laser irradiances below $\sim 3.5 \times 10^{17}\,\mathrm{W}\,\mu\mathrm{m}^2\,\mathrm{cm}^{-2}$, a striking difference between p- and s-polarization is observed. The largest x-ray enhancement is measured by using s-polarized pulses, reaching a factor of ∼38 at $I\lambda^2 \sim 2 \times 10^{17}\,\mathrm{W}\,\mu\mathrm{m}^2\,\mathrm{cm}^{-2}$. In contrast, the x-ray yield obtained by using p-polarized pulses for flat and nanostructured targets is substantially similar. A different enhancement between p- and s-polarization was also obtained by Rajeev *et al* [12] by irradiating rough copper targets with a Ti:Sa laser pulse at intensities in the range 10^{15}–$10^{16}\,\mathrm{W\,cm}^{-2}$ and at an incidence angle of 45°. In that work, the enhancement of x-ray yield in the range 30–300 keV obtained by using s-polarized pulses (∼14) was significantly higher than that obtained by p-pulses (∼3.5). A possible explanation suggested by the authors is the local geometry of laser interaction with the nanostructures, for which a s-polarized pulse can be considered as p at some points of the surface and therefore can drive RA or VH mechanisms. The authors, however, pointed out that some other mechanism may be needed to fully explain their results, since the 'mixing' of p- and s-polarization would also imply a reduction of the x-ray yield obtained by p-polarized pulses, which was not actually found.

Local geometry of laser–plasma interaction, resulting in the mixing of p- and s-polarization on the target surface, could also be considered to explain the present results. According to this interpretation, the large x-ray signal obtained in s-polarization would be therefore produced by the bremsstrahlung emission of hot electrons generated by RA or VH mechanisms in the portions of the surface where the pulse results in a p-like interaction.

Such interpretation, however, is not fully convincing even in our work. First, such a mechanism would suggest an increase of 2nd harmonic emission passing from flat to nanostructured targets when s-polarized pulses are used, since the $2\omega_0$ emission can be considered a signature of the laser interaction at the critical density surface. According to figure 6, the enhancement is not observed. Furthermore, the x-ray emission obtained from nanostructured targets in this 'low intensity' range shows a significant directionality (see figure 5), with a yield which is higher in the plane of incidence for p-polarized pulses and higher in the vertical plane for s-polarized pulses. This result can be hardly explained by RA and VH mechanisms and, at the opposite, suggests the occurrence of TPD process, which could become possible in this intensity range by the lowering of the preplasma threshold, as discussed in the previous section. Figure 4 shows, in fact, that in the case of nanostructured targets a significant preplasma is already produced by the ASE at the lowest irradiance used in the present work.

In this scheme, when s-polarized pulses are used on nanostructured targets, the onset of TPD in the low intensity range results in a strong enhancement of x-rays if compared to the yield provided by flat targets, where no effective mechanism of laser absorption exists. However, in the case

Table 1. Temperature of hot electrons in the energy range 10–25 keV, obtained by the fit of the spectra with a Maxwellian distribution.

	Target			
	Flat silicon, pol P	Flat silicon, pol S	Nanostructured Si, pol P	Nanostructured Si, pol S
$I\lambda^2 < 3.5 \times 10^{17}$ Wμm^2 cm^{-2}	5.4 ± 0.5 keV	3.0 ± 0.5 keV[a]	6.0 ± 0.5 keV	5.0 ± 0.6 keV[a]
$I\lambda^2 > 3.5 \times 10^{17}$ Wμm^2 cm^{-2}	8.6 ± 0.5 keV	8.5 ± 0.5 keV	9.6 ± 0.5 keV	7.8 ± 0.5 keV

[a] In these cases, the number of photons with energies larger than ~10 keV which were detected was very low. For this reason the fit was carried out in the range 8–15 keV.

of p-polarized pulses, the enhancement factor depends on the balance of two processes which tend to produce opposite effects. On one side, the onset of TPD at lower intensities is a source of x-rays as in the s-polarization case; on the other, x-rays produced by RA or VH, which are dominant in flat targets, can be here reduced because TPD drags off laser energy at the quarter critical density. In p-polarization, the detrimental effect of the preplasma on the absorption mechanisms occurring at the critical density, as RA or VH, is suggested by the strong reduction of the $2\omega_0$ emission, which is a factor 20 passing from flat to nanostructured targets, as plotted in figure 6. These two opposite effects seem to balance in the present conditions producing a similar x-ray yield for flat and nanostructured targets.

In view of the interpretation given above, the data provided by the CCD used in the single-photon regime are here discussed in more detail, looking at the high-energy tail which is very sensitive to the effect of TPD as demonstrated in earlier studies [43]. The spectra obtained in the range 10–25 keV have been fitted by using a Maxwellian distribution $f(E) \propto E^{1/2} \exp(-E/T_{\rm hot})$ and the relative slopes, obtained in the different experimental conditions, are reported in table 1.

In order to enhance the signal-to-noise ratio, the spectra obtained at irradiances lower than 3.5×10^{17} W μm^2 cm^{-2} have been averaged, as well as those obtained at $I\lambda^2 > 3.5 \times 10^{17}$ W μm^2 cm^{-2}. The sensitivity of the CCD does not allow an efficient detection of x-rays harder than ~25 keV, so that it is not possible to derive information about the temperature of electrons in the high-energy tail of the distribution. For this reason, hard x-rays produced at relativistic intensities by energetic electrons generated by RA or JxB acceleration—given by ponderomotive [44] and Beg's scalings [45], respectively—are not expected to produce a significant effect on the electron temperatures that we measure.

Nonetheless, the exponential fit of the spectra evidences a population of hot electrons with temperatures in the range 5–10 keV. These values can be compared to probe the consistency of our interpretation. Moreover, to the best of our knowledge, no other paper in the literature reported the temperature of hot electrons obtained by TPD with ultrashort laser pulses.

As expected, the temperatures obtained at higher laser irradiances are generally larger than those obtained at lower irradiances. The temperature obtained for flat silicon irradiated by s-polarized pulses at low laser irradiance is much lower than that obtained in the other cases. This is consistent with the absence of high-energy hot electrons, due to the inefficiency of laser absorption. In the same irradiation conditions, nanostructured targets provide more energetic electrons, due to the onset of TPD.

In the conditions where TPD is expected to be dominant, i.e. at high laser intensities and in the case of nanostructured targets also at low laser intensities, the temperatures obtained for s-polarized pulses are generally lower or similar to those obtained by p-pulses. This result is consistent with the directionality of the hot electrons produced. In fact, the highest kinetic energy of the electrons is expected in the plane of laser polarization, where the accelerating electron field of the plasma waves is larger. Therefore, since the CCD is located in the incidence plane, it is able to measure the hardest x-ray flux resulting from TPD only in the case of p-polarization.

Finally, we want to remark that for hot electrons of 10 keV energy emitted along the plasma wave direction, the intensity of the bremsstrahlung emission is expected to peak in the same direction and decreases by a factor 2 at an angle of 40–45°, which justifies the directionality observed.

4. Conclusions

In this work we investigated the effect of nanostructured targets in laser–plasma interaction at intensities in the range 1×10^{17}–2×10^{18} W μm^2 cm^{-2}. Both the effects of laser pulse polarization and of the formation of a preplasma on the x-ray yield are also investigated.

The results show that in the case of flat targets a change of laser absorption regime occurs at approximately the threshold of preplasma formation, i.e. $I\lambda^2 \sim 3.5 \times 10^{17}$ W μm^2 cm^{-2}, which approximately corresponds to an ASE peak intensity around 1.4×10^{10} W μm^2 cm^{-2}. For laser intensities larger than this value, i.e. in the presence of a preplasma of a few microns scale length, laser absorption in the plasma for both p- and s-polarizations appears significantly affected by parametric instabilities, in particular the TPD process. This is proved by the presence of $3/2\omega_0$ harmonic and results in a non-isotropic x-ray emission, produced via bremsstrahlung of suprathermal electrons accelerated in TPD-induced plasma waves. Significantly different is the case of laser–target coupling for laser intensities lower than the threshold, where x-ray emission loses its directionality and becomes much higher in p- than in s-polarization. This is caused by the effectiveness of absorption of p-polarized pulses by Brunel mechanism, while s-polarized pulses are negligibly absorbed.

When nanostructured targets are used, the threshold of preplasma formation drops significantly due to the increase of laser absorptivity. In this case, a transition between different laser absorption regimes is no longer observed (actually, it probably occurs at lower laser intensities not explored here). TPD could be already effective at $I\lambda^2 \sim 10^{17}$ W μm^2 cm^{-2}, which is again suggested by the non isotropicity of x-ray

emission. The onset of TPD at low intensities results in a strong enhancement of the x-ray yield with respect to flat targets, up to a factor of ∼38, when s-polarized pulses are utilized. Differently, a similar yield of x-ray emission is obtained for p-pulses, which could be explained by the balance of the opposite effects produced by the decrease of laser absorption at the critical density and the onset of TPD in the underdense plasma. At irradiances larger than $\sim 3.5 \times 10^{17}$ W μm^2 cm^{-2}, the effect of nanostructures is marginal, resulting in a modest enhancement of the x-ray yield by a factor of ∼1.2–2. The effect of nanostructures and beam polarization on the x-ray yield enhancement is negligible since the structures are destroyed by the ASE of the pulse. The small enhancement could be tentatively explained by the longer plasma scale length obtained with nanostructured targets due to the lower preplasma threshold.

It is worth remarking that other mechanisms of hot electron generation, as for example ponderomotive acceleration, RA or VH, are likely to occur, depending on laser irradiance and preplasma scale length conditions. These phenomena, however, cannot be sufficient to explain the experimental results, and their contribution in terms of x-rays is expected to be dominant at energies higher than those measured here.

Acknowledgments

This work was carried out in the framework of the CNR High Field Photonics Unit (MD.P03.034). The authors acknowledge financial support from the CNR funded Italian research Network 'ELI-Italy (Attoseconds)' and from the PRIN project (contract no. PRIN2012AY5LEL). We also acknowledge contribution from the MIUR-FIRB project 'SPARX' (Sorgente Pulsata Auto-Amplificata di Radiazione X) and the INFN 'Plasma-med' collaboration. Petra Koester also acknowledges support from the Italian Ministry of Health through the project GR-2009-1608935.

References

[1] Bagchi S, Kiran P P, Yang K, Rao A M, Bhuyan M K, Krishnamurthy M and Kumar G R 2011 *Phys. Plasmas* **18** 014502
[2] Chakravarty U, Arora V, Chakera J A, Naik P A, Srivastava H, Tiwari P, Srivastava A and Gupta P D 2011 *J. Appl. Phys.* **109** 053301
[3] Kneip S *et al* 2008 *High Energy Density Phys.* **4** 41–8
[4] Mondal S *et al* 2011 *Phys. Rev.* B **83** 035408
[5] Nishikawa T, Suzuki S, Watanabe Y, Zhou O and Nakano H 2004 *Appl. Phys.* B **78** 885–90
[6] Ovchinnikov A V, Kostenko O F, Chefonov O V, Rosmej O N, Andreev N E, Agranat M B, Duan J L, Liu J and Fortov V E 2011 *Laser Part. Beams* **29** 249–54
[7] Kahaly S, Yadav S K, Wang W M, Sengupta S, Sheng Z M, Das A, Kaw P K and Kumar G R 2008 *Phys. Rev. Lett.* **101** 145001
[8] Kulcsár G, AlMawlawi D, Budnik F W, Herman P R, Moskovits M, Zhao L and Marjoribanks R S 2000 *Phys. Rev. Lett.* **84** 5149–52
[9] Sumeruk H A *et al* 2007 *Phys. Plasmas* **14** 062704
[10] Sumeruk H A, Kneip S, Symes D R, Churina I V, Belolipetski A V, Donnelly T D and Ditmire T 2007 *Phys. Rev. Lett.* **98** 045001
[11] Rajeev P P, Taneja P, Ayyub P, Sandhu A S and Kumar G R 2003 *Phys. Rev. Lett.* **90** 115002
[12] Rajeev P P, Banerjee S, Sandhu A S, Issac R C, Tribedi L C and Kumar G R 2002 *Phys. Rev.* A **65** 052903
[13] Cao L, Gu Y, Zhao Z, Cao L, Huang W, Zhou W, He X T, Yu W and Yu M Y 2010 *Phys. Plasmas* **17** 043103
[14] Chatterjee G *et al* 2012 *Phys. Rev. Lett.* **108** 235005
[15] Singh P K, Chakraborty I, Chatterjee G, Adak A, Lad A D, Brijesh P, Ayyub P and Kumar G R 2013 *Phys. Rev. ST Accel. Beams* **16** 063401
[16] Zhao Z *et al* 2010 *Phys. Plasmas* **17** 123108
[17] Rajeev P P, Ayyub P, Bagchi S and Kumar G R 2004 *Opt. Lett.* **29** 2662
[18] Kreibig U and Vollmer M 1995 *Optical Properties of Metal Clusters* (Berlin: Springer)
[19] Nikbakht M and Mahdieh M H 2012 *J. Eur. Opt. Soc. Rapid Publ.* **7** 12025
[20] Chakravarty U, Arora V, Naik P A, Chakera J A, Srivastava H, Srivastava A, Varma G D, Kumbhare S R and Gupta P D 2012 *J. Appl. Phys.* **112** 053301
[21] Dhareshwar L J *et al* 2010 *J. Phys. Conf. Ser.* **244** 022018
[22] Purvis M A *et al* 2013 *Nature Photon.* **7** 796–800
[23] Giulietti D, Biancalana V, Batani D, Giulietti A, Gizzi L and Nocera L 1991 *Lett. Nuovo Cimento* **13** 845–58
[24] Veisz L, Theobald W, Feurer T, Schwoerer H, Uschmann I, Renner O and Sauerbrey R 2004 *Phys. Plasmas* **11** 3311–23
[25] Tarasevitch A, Dietrich C, Blome C, Sokolowski-Tinten K and von der Linde D 2003 *Phys. Rev.* E **68** 026410
[26] Li C *et al* 2011 *Phys. Rev.* E **84** 036405
[27] Dong Q L, Zhang J and Teng H 2001 *Phys. Rev.* E **64** 026411
[28] Labate L, Koester P, Levato T and Gizzi L A 2012 *Rev. Sci. Instrum.* **83** 103504
[29] Labate L, Levato T, Galimberti M, Giulietti A, Giulietti D, Sanna M, Traino C, Lazzeri M and Gizzi L A 2008 *Nucl. Instrum. Meth. Phys. Res.* A **594** 278
[30] Levato T, Labate L, Galimberti M, Giulietti A, Giulietti D and Gizzi L A 2008 *Nucl. Instrum. Meth. Phys. Res.* A **592** 346
[31] Knoll G F 2000 *Radiation Detection and Measurement* (New York: John Willey)
[32] Pert G J 1989 *J. Plasma Phys.* **41** 263
[33] Marinica D C, Kazansky A K, Nordlander P, Aizpurua J and Borisov A G 2012 *Nano Lett.* **12** 1333–9
[34] Baffigi F, Cristoforetti G, Fulgentini L, Giulietti A, Koester P, Labate L, Gizzi L A 2014 *Phys. Plasmas* submitted
[35] Ebrahim N A, Baldis H A, Joshi C and Benesch R 1980 *Phys. Rev. Lett.* **45** 1179–82
[36] Figueroa H, Joshi C, Azecgi H, Ebrahim N A and Estabrook K 1984 *Phys. Fluids* **27** 1887–96
[37] Chen L M, Zhang J, Li Y T, Teng H, Liang T J, Sheng Z M, Dong Q L, Zhao L Z, Wei Z Y and Tang X W 2001 *Phys. Rev. Lett.* **87** 225001
[38] Zhang J, Sheng Z M, Li Y T, Qiu Y, Jin Z and Teng H 2004 *Phys. Rev.* E **69** 046408
[39] Zhang J, Li Y T, Sheng Z M, Wei Z Y, Dong Q L and Lu X 2005 *Appl. Phys.* B **80** 957
[40] Sheng Z M, Li Y T, Zhang J and Veisz L 2005 *IEEE Trans. Plasma Sci.* **33** 486
[41] Brunel F 1987 *Phys. Rev. Lett.* **59** 52
[42] Gizzi L A, Giulietti D, Giulietti A, Audebert P, Bastiani S, Geindre J P and Mysyrowicz A 1996 *Phys. Rev. Lett.* **76** 2278–81
[43] Gizzi L, Batani D, Biancalana V, Giulietti A and Giulietti D 1992 *Laser Part. Beams* **10** 65–74
[44] Wilks S C and Kruer W L 1997 *IEEE J. Quantum Electron.* **33** 1954
[45] Beg F N, Bell A R, Dangor A E, Danson C N, Fews A P, Glinsky M E, Hammel B A, Lee P, Norreys P A and Tatarakis M 1997 *Phys. Plasmas* **4** 447